THE JOURNAL OF BIOLOGICAL CHEMISTRY VOL. 284, NO. 13, pp. 8846–8854, March 27, 2009

Functional Interactions between Distinct Sodium Channel Cytoplasmic Domains through the Action of Calmodulin*

Received for publication, September 4, 2008, and in revised form, January 12, 2009 Published, JBC Papers in Press, January 26, 2009, DOI 10.1074/jbc.M806871200

Franck Potet[‡1], Benjamin Chagot[§¶], Mircea Anghelescu[‡], Prakash C. Viswanathan[‖], Svetlana Z. Stepanovic[‡], Sabina Kupershmidt[‡], Walter J. Chazin[§¶], and Jeffrey R. Balser[‡**‡‡]**

*From the Departments of [‡]Anesthesiology, **Pharmacology, [§]Medicine, [§]Biochemistry, and [‡‡]Chemistry and [¶]Center for Structural Biology, Vanderbilt University, Nashville, Tennessee 37232 and the [‖]Cardiovascular Institute, University of Pittsburgh Medical Center, Pittsburgh, Pennsylvania 15213*

Sodium channels are fundamental signaling molecules in excitable cells, and are molecular targets for local anesthetic agents and intracellular free Ca^{2+} ($[Ca^{2+}]_i$). Two regions of $Na_V1.5$ have been identified previously as $[Ca^{2+}]_i$-sensitive modulators of channel inactivation. These include a C-terminal IQ motif that binds calmodulin (CaM) in different modes depending on Ca^{2+} levels, and an immediately adjacent C-terminal EF-hand domain that directly binds Ca^{2+}. Here we show that a mutation of the IQ domain (A1924T; Brugada Syndrome) that reduces CaM binding stabilizes $Na_V1.5$ inactivation, similarly and more extensively than even reducing $[Ca^{2+}]_i$. Because the DIII-DIV linker is an essential structure in $Na_V1.5$ inactivation, we evaluated this domain for a potential CaM binding interaction. We identified a novel CaM binding site within the linker, validated its interaction with CaM by NMR spectroscopy, and revealed its micromolar affinity by isothermal titration calorimetry. Mutation of three consecutive hydrophobic residues (Phe^{1520}–Ile^{1521}–Phe^{1522}) to alanines in this CaM-binding domain recapitulated the electrophysiology phenotype observed with mutation of the C-terminal IQ domain: $Na_V1.5$ inactivation was stabilized; moreover, mutations of either CaM-binding domain abolish the well described stabilization of inactivation by lidocaine. The direct physical interaction of CaM with the C-terminal IQ domain and the DIII–DIV linker, combined with the similarity in phenotypes when CaM-binding sites in either domain are mutated, suggests these cytoplasmic structures could be functionally coupled through the action of CaM. These findings have bearing upon Na^+ channel function in genetically altered channels and under pathophysiologic conditions where $[Ca^{2+}]_i$ impacts cardiac conduction.

Voltage-gated sodium (Na^+) channels underlie the rapid upstroke and propagation of action potentials in excitable cells and are therefore important targets for drug therapy in disorders of the nervous system as well as muscle. The cardiac Na^+ channel ($Na_V1.5$, SCN5A) is the primary molecular species generating cardiac rhythm and has been implicated in various forms of sudden cardiac death due to ventricular fibrillation (1).

In this study, the effects of mutations within two CaM-binding domains, one in the $Na_V1.5$ C terminus, and one in the DIII–DIV linker (see schematic, Fig. 3*B*) were studied in low or high $[Ca^{2+}]$ by comparing steady-state availability of mutants to wild-type (WT)[2] $Na_V1.5$. The availability of both variants is greatly influenced by $[Ca^{2+}]_i$, and involves channel structures that are important in channel inactivation. Inactivation, a highly voltage-dependent conformational change elicited by depolarization, truncates the duration of channel opening and terminates Na^+ conduction.

Site-directed mutagenesis of cloned Na^+ channel isoforms has shown that the cytoplasmic linker between homologous domains III and IV (DIII–DIV linker, see Fig. 3*B*) is a crucial component of the channel inactivation machinery (2, 3). Nonconservative mutation of DIII–DIV linker amino acid residues disrupts inactivation; however, this disruption is partly repaired by addition of local anesthetics (LA) (4). The action of LA molecules on $Na_V1.5$ hinges critically upon transitions among distinct conformational states (2, 3). LA compounds "stabilize" Na^+ channel inactivation through an allosteric effector mechanism, *i.e.* they shift the conformational state equilibrium from rested to inactivated states (4). Finally, a number of mutations in the Na^+ channel C terminus also modulate both inactivation and LA action, suggesting the C terminus functionally interacts with the DIII–DIV linker during inactivation (5, 6).

The Brugada syndrome, a rare autosomal dominant disorder of idiopathic ventricular fibrillation, has been attributed to alterations in Na^+ channel function arising from mutations in $Na_V1.5$ (7). Functional analysis of recombinant Na^+ channels that carry these mutations, particularly those in the C terminus (8–10), reveals familiar changes in inactivation that resemble the inactivation-stabilizing effects of LA agents.

Intracellular free Ca^{2+} concentration ($[Ca^{2+}]_i$) fluctuates as a function of excitation-contraction coupling, and when cells are subjected to ischemia or traumatic injury (11). $Na_V1.5$ exhibits sensitivity to $[Ca^{2+}]_i$ in a complex manner through the dual action of an "IQ-type" calmodulin (CaM)-binding domain

* This work was supported, in whole or in part, by National Institutes of Health NIGMS Grant GM56307-11. The costs of publication of this article were defrayed in part by the payment of page charges. This article must therefore be hereby marked "*advertisement*" in accordance with 18 U.S.C. Section 1734 solely to indicate this fact.

[1] To whom correspondence should be addressed: 2213 Garland Ave., Langford P445 MRB IV, Nashville, TN 37232-0413. Fax: 615-936-0456; E-mail: franck.potet@vanderbilt.edu.

[2] The abbreviations used are: WT, wild type; LA, local anesthetics; CaM, calmodulin; HSQC, heteronuclear single quantum coherence; t-BHP, *t*-butyl hydroperoxide; MES, 4-morpholineethanesulfonic acid; BisTris, 2-[bis(2-hydroxyethyl)amino]-2-(hydroxymethyl)propane-1,3-diol; ITC, isothermal titration calorimetry; BAPTA, 1,2-bis(2-aminophenoxy)ethane-*N*,*N*,*N*′,*N*′-tetraacetic acid.

in the C terminus (8, 12, 13). This domain exhibits multiple CaM binding modes, which are influenced by $[Ca^{2+}]_i$ (14), as well as an interaction with a C-terminal EF-hand domain that directly binds the IQ domain (15). In conditions where $[Ca^{2+}]_i$ is elevated, interaction between the EF-hand and the IQ domain "destabilizes" channel inactivation, *i.e.* reduces the likelihood channels will occupy the inactivated state at the resting membrane potential (14). Hence, the effects of increasing $[Ca^{2+}]_i$ on Na^+ channel inactivation are opposite to those of LA drugs.

Using varying $[Ca^{2+}]_i$ and LA as molecular probes, we show here that CaM binding to specific domains within the C terminus and DIII–DIV linker both influence inactivation of $Na_V1.5$. Patch-clamp studies revealed that the effects of lowering $[Ca^{2+}]_i$ can be reproduced by site-directed mutagenesis in the C-terminal IQ domain. We also used NMR to show a direct interaction between CaM and the DIII–DIV linker, and sequence analysis and isothermal calorimetry revealed an embedded high affinity CaM-binding domain in the linker region. Mutation within this site, like the IQ domain, recapitulated the effects of lowering $[Ca^{2+}]_i$ and abolished the stabilization of inactivation by LA in patch clamp experiments, suggesting the C-terminal and DIII–DIV linker CaM-binding domains may be functionally coupled.

These results provide important insights into the molecular mechanisms that modulate inactivation through Ca^{2+}-regulated CaM binding to the $Na_V1.5$ C terminus and DIII–DIV linker. CaM interaction with the inactivation mechanism of $Na_V1.5$ may provide a novel therapeutic strategy for conditions caused by sodium channel dysfunction in the heart and brain.

MATERIALS AND METHODS

Plasmid Construction, Cell Culture, and Transfection—Site-directed mutagenesis was carried out on SCN5A cDNA subcloned into GFP-IRES vector for the bicistronic expression of the channel protein and green fluorescent protein, as described previously (16). Mutation sites and the whole gene sequence were verified by resequencing. Cultured cells (tsA201) were transiently transfected with 1.5 μg of either wild type or mutant (A1924T) cDNA. Green fluorescent cells were selected for electrophysiological analysis 24 h later. The cells were maintained in tissue culture dishes using Dulbecco's modified Eagle's medium with 10% fetal bovine serum and 1% penicillin-streptomycin. Cells were transfected with Lipofectamine^{TM} (Invitrogen) according to the manufacturer's instructions.

Electrophysiology—I_{Na} was recorded at 22 °C and analyzed as described (16). The voltage-clamp protocols used are shown in Fig. 1. A Boltzmann function ($I = 1/[1 + \exp(V_t - V_{½})/\delta)]$) was fitted to the availability curves to determine the membrane potential eliciting half-maximal inactivation ($V_{½}$), where δ is the slope factor. The pipette solution used to approximate zero $[Ca^{2+}]_i$ contained (in mM): 10 sodium fluoride, 100 caesium fluoride, 20 CsCl, 20 BAPTA, 10 HEPES, adjusted to pH 7.35 with CsOH. For high $[Ca^{2+}]_i$ (1 μM free Ca^{2+}), 1 mM BAPTA was used with 0.9 mM Ca^{2+}. The extracellular (bath) recording solution contained (in mM): 145 NaCl, 4 KCl, 1 $MgCl_2$, 10 HEPES, and 1.8 $CaCl_2$, adjusted to pH 7.35 with CsOH. To avoid the time-dependent shift of the I_{Na} availability curve commonly observed during patch clamp experiments, voltage-dependent inactivation was assessed within 2 min after rupture of the membrane. Due to this experimental set-up, we did not attempt to compare conditions with and without lidocaine in the same cell, and instead utilized cell-to-cell comparisons. Patch clamp measurements are presented as the mean ± S.E. Comparisons were made using Student's *t* test, with $p < 0.05$ considered significant.

Protein Production and Purification—The DIII–DIV linker (Asp^{1471}–Asp^{1523}) was expressed from pET15b constructs in BL21(DE3) strain cells at 37 °C in LB media. After centrifugation, cells pellets were resuspended in 50 mM Tris (pH 7.5), 50 mM NaCl, and 5 mM β-mercaptoethanol (lysis buffer). The cells were lysed by sonication and concentrated. Filtered cell lysate was loaded onto a Ni^{2+}-affinity column equilibrated with lysis buffer, washed, and the protein was eluted with a gradient of 50 mM Tris (pH 7.5), 50 mM NaCl, 5 mM β-mercaptoethanol, and 300 mM imidazole. The protein was cleaved from the His tag using thrombin, then purified over a second Ni^{2+} column. A final purification step involved ion exchange chromatography, with the protein eluted in a gradient from lysis buffer into 50 mM Tris (pH 7.5), 1 M NaCl, and 5 mM β-mercaptoethanol.

CaM was subcloned into the in-house pBG100 vector, which expresses the native protein of interest. CaM was expressed in BL21(DE3) host cells at 37 °C in LB media or M9 media supplemented with $^{15}NH_4Cl$ for ^{15}N labeling. The protein was purified over a phenyl-Sepharose column (17). CaM concentration was determined by A_{276}, using an extinction coefficient of $\epsilon = 3{,}006\ M^{-1}\ cm^{-1}$.

Nuclear Magnetic Resonance—^{15}N-^{1}H heteronuclear single quantum coherence (HSQC) NMR spectra were recorded at 37 °C on a 500 MHz Bruker AVANCE spectrometer equipped with a cryoProbe. CaM and the DIII–DIV linker were dialyzed against 5 mM MES, 10 mM BisTris (pH 6.5), 5 mM $CaCl_2$, and 0.1 mM NaN_3. NMR titrations were performed in a solution of 200 μM ^{15}N-CaM, adding increasing amounts of DIII–DIV linker to final concentrations of 50, 100, 200, and 400 μM. Chemical shifts deposited for CaM in the BioMagResBank (code 6541) (18) were used for resonance assignments. Spectra were processed using NMRPipe (19) and analyzed with Sparky (T. D. Goddard and D. G. Kneller, SPARKY 3, University of California, San Francisco, CA).

Isothermal Titration Calorimetry—ITC measurements were carried out with a VP-ITC MicroCalorimeter (MicroCal, Inc., Northampton, MA). Titration experiments were performed in 50 mM Tris (pH 7.5) containing 50 mM NaCl and 1 mM $CaCl_2$. Protein and peptide were dialyzed against this buffer. DIII–DIV or peptide fragments at 42–62 μM in the calorimetric cell was titrated by a series of injections of CaM (649–795 μM). The binding isotherms, ΔH *versus* molar ratio, were analyzed with a single-site binding model using MicroCal Origin software. The association constant, k_a was directly obtained from the fit to the data points and converted to the dissociation constant K_d ($K_d = 1/k_a$).

Peptide Synthesis—Peptides were synthesized by Sigma-Genosys. Peptides were purified by reversed-phase high performance liquid chromatography and analyzed by mass spectrometry to confirm purity and molecular weight.

RESULTS

C-terminal Ca^{2+}-sensing Domains Mediate Responses to $[Ca^{2+}]_I$, CaM, and LA in an Interdependent Fashion—Whole cell Na^+ current (I_{Na}) was recorded in voltage-clamped tsA201 (HEK) cells transiently transfected with WT $Na_V1.5$ cDNA. Voltage-dependent inactivation was assessed by plotting I_{Na} during an activating pulse to −20 mV (Fig. 1*A*) as a function of the preceding membrane potential. The voltage-dependent availability curves reflect the fraction of channels available to open and thus the proportion of channels *not* inactivated at each membrane potential. A right shift in the curve indicates a larger number of channels available to open at any given voltage, whereas a left shift indicates the opposite. Brief clamp pulses of 50 ms were utilized to exclude slowly developing inactivation processes that involve extracellular domains (20). Fig. 1*A* demonstrates that the likelihood of voltage-dependent inactivation of $Na_V1.5$ is reduced at any given voltage by increasing $[Ca^{2+}]_i$, as such, the *availability* of channels to open is enhanced (14, 15). Hence, in elevated (1 μM free) $[Ca^{2+}]_i$, I_{Na} is increased when elicited from a voltage near the cardiac cell resting potential (compare −80 mV small traces, Fig. 1*B*). At this $[Ca^{2+}]_i$, lidocaine had an opposing effect, left-shifting the voltage-dependent inactivation curve of $Na_V1.5$. This classic effect of the LA reduces $Na_V1.5$ channel availability and I_{Na} at voltages near the cell resting potential (Fig. 1*B*), consistent with a stabilizing effect on inactivation (21, 22). Table 1 provides statistical comparisons of the voltage at which channels studied in various conditions are 50% inactivated ($V_{½}$).

Remarkably, when $[Ca^{2+}]_i$ was clamped to low-nanomolar concentrations using 20 mM BAPTA, we found that the lidocaine-induced left-shift in the voltage dependence of inactivation was greatly reduced (Fig. 1*A*), suggesting that sensitivity of $Na_V1.5$ inactivation to LA and Ca^{2+}-CaM are interdependent (compare *open symbols* to *filled triangles*, Fig. 1*A*). Neither changing $[Ca^{2+}]_i$ nor exposure to lidocaine altered the rate of $Na_V1.5$ inactivation (Fig. 1*B*; time constants for I_{Na} decay provided in legend). Furthermore, use-dependent lidocaine action linked to kinetically slower inactivation processes (20, 23) was not altered by changing $[Ca^{2+}]_i$ (10 Hz pulse train, Fig. 1*C*), suggesting the effects of $[Ca^{2+}]_i$ are specific for the voltage dependence of the fast, primary inactivation process. Stabilization of fast inactivation through lidocaine action largely involves cytoplasmic structures such as the C terminus and interdomain linkers, and is manifest as an equilibrium shift with more channels inactivating from closed, rested states (6). In contrast, the development of use-dependent block (Fig. 1*C*) has a distinctive pharmacology and structural relationships involving the amino acid residues lining the outer pore (20).

The Na^+ channel variant A1924T, isolated from a Brugada syndrome patient exhibiting the

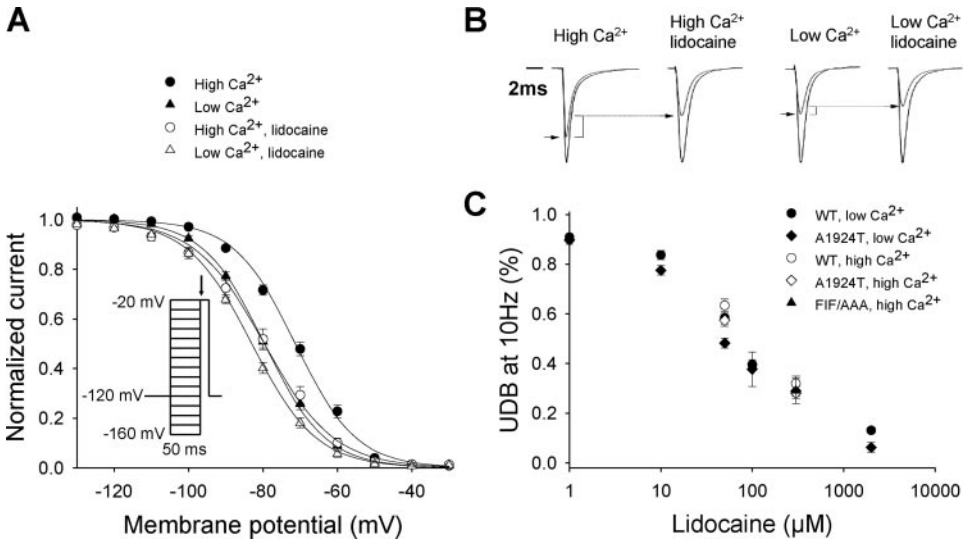

FIGURE 1. **Effects of lidocaine on $Na_V1.5$ in the presence and absence of Ca^{2+}.** *A*, voltage dependence of inactivation in cells expressing $Na_V1.5$ in the absence or presence of 300 μM lidocaine in high (1 μM) $[Ca^{2+}]_i$ or a nominally Ca^{2+}-free solution (plus 20 mM BAPTA). In high $[Ca^{2+}]_i$, $V_{½}$ was −71.3 ± 0.9 mV (●; $n = 24$) in the absence, and −79.6 ± 1.7 mV (○; $n = 15$) in the presence of lidocaine ($p < 0.001$). In low $[Ca^{2+}]_i$, $V_{½}$ was −79.6 ± 1.0 mV (▲; $n = 22$) in the absence and −83.0 ± 0.8 mV (Δ; $n = 18$) in the presence of lidocaine ($p < 0.05$). *Inset*, voltage clamp protocol used to assess the voltage-dependent inactivation. Current amplitude measured during an activating pulse to −20 mV (*arrow*) as a function of the preceding membrane potential (from −160 to −20 mV) were used to construct the steady-state inactivation curve. *B*, representative currents in high and low $[Ca^{2+}]_i$ in the presence or absence of lidocaine. For each condition, the largest current traces show recordings obtained at −20 mV following a prepulse to −160 mV and *smaller lines* show recordings obtained after a prepulse at −80 mV. Decay rates of the currents at −20 mV after a prepulse at −160 mV were fit with the sum of two exponential components. The rates of current decay measured in high $[Ca^{2+}]_i$ ($\tau_f = 0.55 \pm 0.02$; $\tau_s = 2.7 \pm 0.14$), high $[Ca^{2+}]_i$ plus lidocaine ($\tau_f = 0.59 \pm 0.06$; $\tau_s = 2.72 \pm 0.33$), in low $[Ca^{2+}]_i$ ($\tau_f = 0.53 \pm 0.02$; $\tau_s = 2.68 \pm 0.2$) and low $[Ca^{2+}]_i$ plus lidocaine ($\tau_f = 0.51 \pm 0.03$; $\tau_s = 2.48 \pm 0.35$) were not different (p = NS). *C*, dose-response curve for use-dependent block of $Na_V1.5$ WT, A1924T, and FIF/AAA at pulse number 50. Use dependence was induced by depolarizing channels to 10 mV for 20 ms from a holding potential of 120 mV at 10 Hz.

TABLE 1

Effects of $[Ca^{2+}]_i$ and lidocaine on the $V_{½}$ of steady-state inactivation for $Na_V1.5$

WT, A1924T and FIF/AAA. All data represent the mean ± S.E. The $V_{½}$ for WT, A1924T, and FIF/AAA in high $[Ca^{2+}]_i$ were not different.

	WT	A1924T	FIF/AAA
1 μM Ca^{2+}	−71.3 ± 0.9 mV	−74.7 ± 1.9 mV	−73.7 ± 1.0 mV
1 μM Ca^{2+} + lidocaine	−79.6 ± 1.7 mV[a]	−75.4 ± 1.4 mV[b]	−74.1 ± 0.6 mV[b]
20 mM BAPTA	−79.6 ± 1.0 mV[c]	−87.4 ± 1.2 mV[c,d]	−85.9 ± 0.9 mV[c,d]
20 mM BAPTA+ lidocaine	−83.0 ± 0.8 mV[a,c]	−85.5 ± 1.5 mV[b,c]	

[a] $p < 0.05$ *versus* same condition without lidocaine.
[b] p = NS *versus* same condition without lidocaine.
[c] $p < 0.05$ *versus* same condition as in 1 μM Ca^{2+}.
[d] $p < 0.05$ *versus* WT + 20 mM BAPTA.

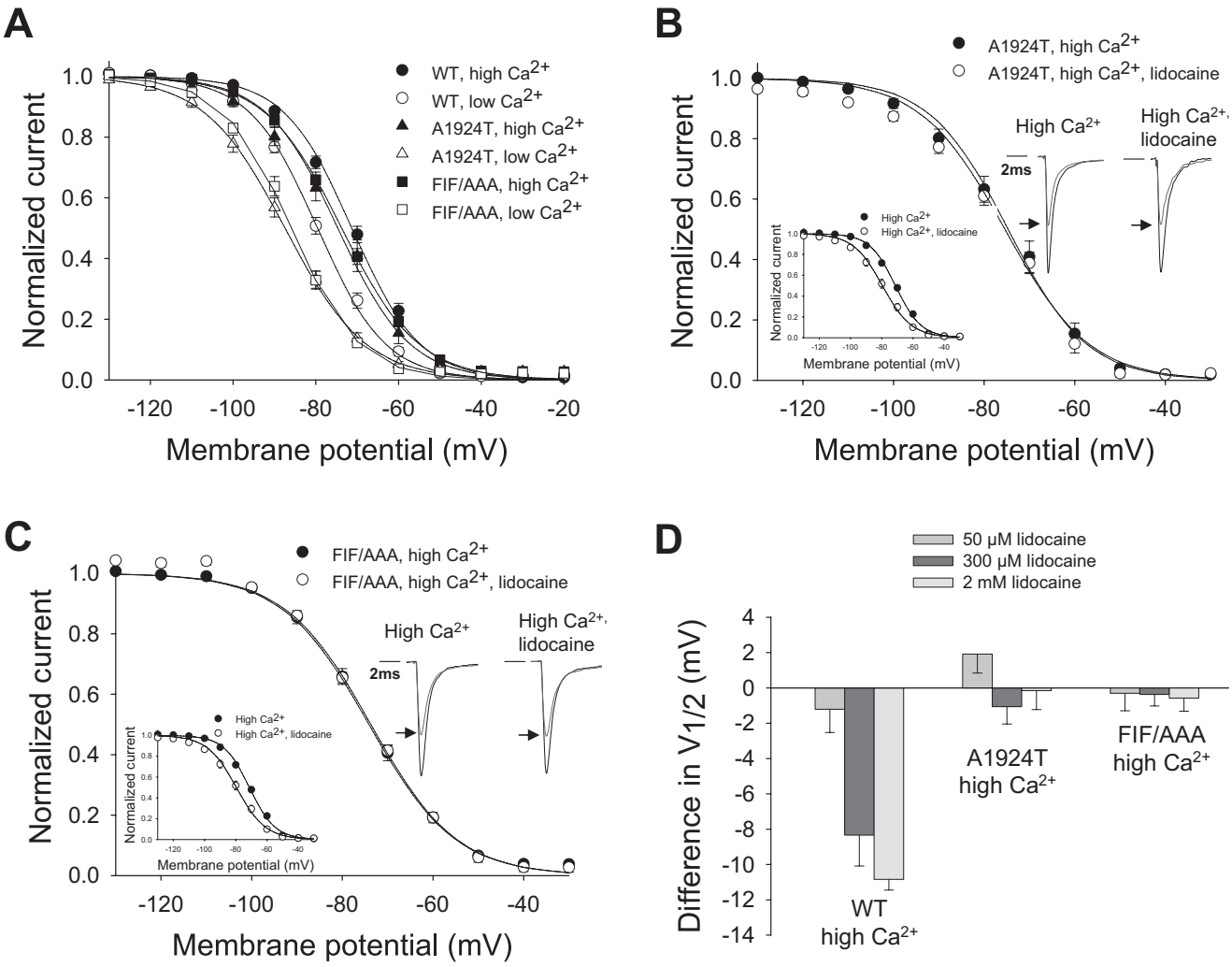

FIGURE 2. **CaM-binding domains in the C terminus and DIII--DIV linker region control the effects of lidocaine on $Na_V1.5$ steady-state availability.** *A*, voltage dependence of inactivation in cells expressing WT, A1924T, or FIF/AAA (1.5 μg cDNA each) in low or high $[Ca^{2+}]_i$. In high $[Ca^{2+}]_i$, WT, A1924T, and FIF/AAA $V_{1/2}$ of inactivation were not significantly different (-71.3 ± 0.9 mV (●; $n = 24$), -74.7 ± 1.9 mV (▲; $n = 13$), and -73.7 ± 1.0 mV (■; $n = 13$), respectively (p = NS)). In low $[Ca^{2+}]_i$, the $V_{1/2}$ of inactivation of WT significantly differed from A1924T and FIF/AAA (-79.6 ± 1.0 mV (○; $n = 22$), -87.4 ± 1.2 mV (△; $n = 11$; $p < 0.05$), and -85.9 ± 0.9 mV (□; $n = 9$; $p < 0.05$), respectively). *B*, $V_{1/2}$ for A1924T in the absence or presence of lidocaine in high $[Ca^{2+}]_i$ was -74.7 ± 1.9 mV (●; $n = 13$) and -75.4 ± 1.4 mV (○; $n = 9$), respectively (p = NS). *Left inset*, voltage-dependent inactivation for WT $Na_V1.5$ under the same conditions. *Right inset*, representative current traces in 1 μM $[Ca^{2+}]_i$, in the presence (*left*) or absence (*right*) of lidocaine. *Black traces* show currents obtained at -20 mV after a prepulse at -160 mV, the *small lines* show the currents obtained after a prepulse at -80 mV. Decay rates of the currents at -20 mV after a prepulse to -160 mV were fit with the sum of two exponential components. The biexponential decay rates of A1924T in high $[Ca^{2+}]_i$ in the absence ($\tau_f = 0.51 \pm 0.02$; $\tau_s = 2.46 \pm 0.17$) and presence of lidocaine ($\tau_f = 0.57 \pm 0.05$; $\tau_s = 2.42 \pm 0.26$) were not different (p = NS). *C*, voltage-dependent inactivation of $Na_V1.5$ FIF/AAA in the absence or presence of lidocaine in high $[Ca^{2+}]_i$. $V_{1/2}$ was -73.7 ± 1.0 mV (●; $n = 13$) in the absence and -74.1 ± 0.6 mV (○; $n = 5$) in the presence of lidocaine (p = NS). *Left inset*, same as in *B*. *Right inset*, representative $Na_V1.5$ FIF/AAA currents in 1 μM Ca_i, in the presence (*left*) or absence (*right*) of lidocaine. Color coding is as described in *B*. The biexponential decay rates of $Na_V1.5$ FIF/AAA in high $[Ca^{2+}]_i$ in the absence ($\tau_f = 0.54 \pm 0.03$; $\tau_s = 2.7 \pm 0.33$), and presence of lidocaine ($\tau_f = 0.52 \pm 0.05$; $\tau_s = 2.27 \pm 0.42$) were not different (p = NS). *D*, shifts in the $V_{1/2}$ of steady-state inactivation of $Na_V1.5$ WT, A1924T, and FIF/AAA with or without 50, 300, or 2000 μM lidocaine in high $[Ca^{2+}]_i$ from *B* and *C* and Fig. 1*A*.

attendant diagnostic changes in the surface electrocardiogram, resides in the C-terminal IQ domain of $Na_V1.5$ and reduces the CaM affinity of the IQ motif 10-fold (14). To probe whether the effect of changing $[Ca^{2+}]_i$ is mediated through CaM binding to $Na_V1.5$, we examined A1924T in varying Ca^{2+} and lidocaine conditions. As shown in Fig. 2*A* and Table 1, in low $[Ca^{2+}]_i$ the $V_{½}$ of inactivation for WT shifts to the left (compare *open* and *filled circles*). The $V_{½}$ of inactivation for the A1924T mutant also shifts to the left in response to lowering $[Ca^{2+}]_i$ (compare *filled* and *open triangles*), indicating that Ca^{2+} responsiveness of the EF-hand motif is intact. However, the A1924T mutant experiences a left-shift that goes beyond what is observed for WT (compare *open circles* and *triangles*; see also Table 1). This "super-shift" suggests that in WT channels, and in low $[Ca^{2+}]_i$, CaM binding plays an important role in limiting the development of inactivation. In high $[Ca^{2+}]_i$ the mutant and WT channels have nearly identical voltage-dependent inactivation profiles, and the kinetics of the mutant channel are also not changed (see Fig. 2*B*, *insets*). Moreover, the voltage dependence of A1924T inactivation was no longer sensitive to lidocaine, even at high $[Ca^{2+}]_i$ (Fig. 2, *B* and *D*, and Table 1). As summarized in Fig. 2*D*, the voltage dependence of A1924T inactivation was remarkably insensitive to lidocaine (concentrations up to 2 mM were tested). In contrast, the dose dependence of use-dependent block of A1924T was indistinguishable from WT (Fig. 1*C*). These results suggest that CaM binding to the IQ domain

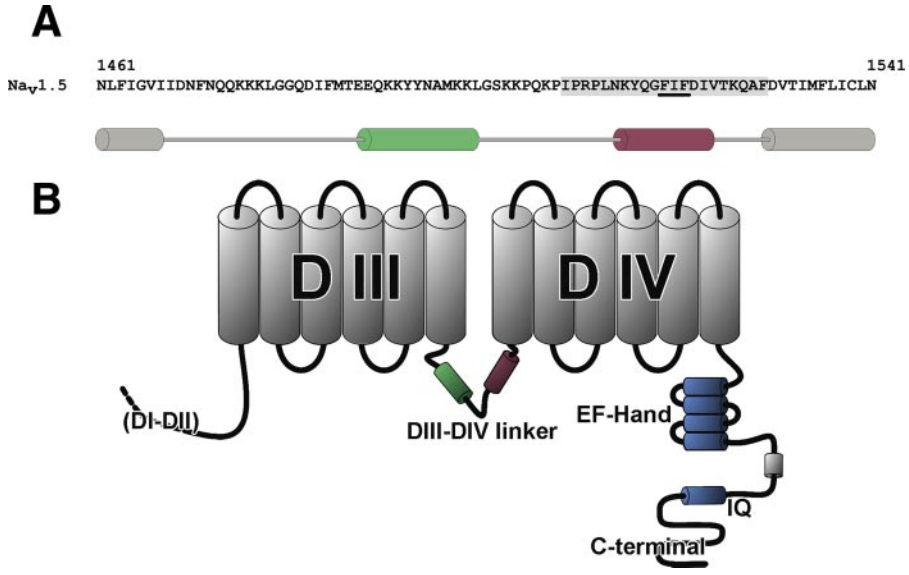

FIGURE 3. **Schematic diagram of hH1 domains and sequence details.** *A*, sequence and secondary structure prediction of the DIII–DIV linker. The ^{1520}FIF^{1522} region is *underlined*, the CaM-binding domain is highlighted in *gray*. *Gray cylinders* represent the transmembrane regions and *green* and *violet cylinders* represent predicted helical regions of the DIII–DIV linker. *B*, schematic representation of the DIII, DIV, and C-terminal domains of hH1. *DI* and *DII* are not represented, EF-hand domain, and IQ motif of the C-terminal domain are colored *blue*. Predicted helical regions of the DIII–DIV linker are colored as in *A*.

in low Ca^{2+} is key to controlling fast inactivation. Given that $[Ca^{2+}]_i$ regulates CaM binding to the IQ domain (14), we conclude that the functional effects of CaM binding to the C-terminal IQ domain are influenced by $[Ca^{2+}]_i$, and involve inactivation structures that are also responsive to LA.

Although these results suggest that CaM binding influences LA action on inactivation, a potential alternative explanation is that A1924T modifies LA affinity for the rested (closed) state. We measured the effects of lidocaine on I_{Na} under conditions where inactivation would be negligible, by holding the membrane at −120 mV. At this potential, inhibition by lidocaine should solely be a function of resting state affinity. Under these conditions, lidocaine block of WT and A1924T were identical (percent inhibition of peak current measured at −20 mV using 300 μM lidocaine was 41 ± 2 and 38 ± 7%, $n = 5$, p = NS, respectively), indicating that the rested state affinity was not altered in the mutant.

A CaM-binding Domain in the DIII–DIV Linker Has Corresponding Effects on Inactivation Gating—Although the C-terminal region is involved in regulation of inactivation by CaM, the DIII–DIV linker is the primary structure responsible for Na^+ channel fast inactivation. In addition, the DIII–DIV linker has recently been implicated as a site for CaM interaction (13, 14, 24). Moreover, it has been proposed that CaM is required to stabilize the interaction of the C terminus with the DIII–DIV linker (13). These observations suggest a direct role for CaM in modulating the action of the DIII–DIV linker in the inactivation of $Na_V1.5$.

To test for direct physical interaction, NMR chemical shift perturbation analysis was performed using ^{15}N-enriched CaM. Fig. 4*A* shows an overlay of ^{15}N-^{1}H HSQC spectra acquired for ~200 μM Ca^{2+}-loaded CaM with concentrations up to ~400 μM DIII–DIV linker added to the solution. The highlighted region of the spectrum shown in the figure was selected to show perturbed resonances in the well resolved downfield region of the spectrum. The observation of a change in an NMR signal over the course of the titration is an extremely sensitive reporter on inter-molecular interactions and structural perturbations. Hence, these data demonstrate the existence of a direct physical interaction between CaM and the DIII–DIV linker. There are almost no differences in the NMR spectrum with ~200 and ~400 μM DIII–DIV linker added, which indicates that the titration is complete at a 1:1 ratio. Note that only a subset of the NMR signals is affected throughout the course of titration, which indicates a specific binding event is being monitored. To quantify the affinity of Ca^{2+}-loaded CaM for the DIII–DIV linker, isothermal titration calorimetry (ITC) was used to measure heat evolution over the course of a titration (Fig. 4*B*). Fitting of the data to the standard binding equation provided a dissociation constant (K_d) of 0.6 μM and a stoichiometry of 1.

To search for the CaM binding site in the DIII–DIV linker, the sequence of $Na_V1.5$ was analyzed using the Calmodulin Target Data base (25). A CaM-binding domain was predicted at the C-terminal end of the DIII–DIV linker just as it re-enters the membrane (Fig. 3*A*, *shaded gray*). To validate this prediction, a corresponding 21-residue peptide was synthesized and its affinity for Ca^{2+}-bound CaM was measured using ITC (Fig. 4*C*). Fitting of this data to a standard single site binding equation provides a K_d of 8.2 μM.

To further localize the determinants of this interaction, specific mutations were introduced into the CaM-binding domain within the DIII–DIV linker. Interaction between CaM and its binding partners is often mediated by hydrophobic interactions (25). Of particular note in the DIII–DIV CaM-binding domain are three consecutive hydrophobic residues (Phe^{1520}–Ile^{1521}–Phe^{1522}) (Fig. 3, *underlined residues*). Mutations of these residues to alanines (FIF/AAA) were found to decrease the affinity of the CaM-binding domain peptide ~10-fold; an ITC experiment performed under identical conditions to that used for the wild-type peptide gave a K_d of 66 μM (Fig. 4*D*). These results suggest that the FIF motif plays a significant role in mediating the interaction between CaM and the DIII–DIV linker of $Na_V1.5$.

To test the functional importance of the CaM-binding domain within the DIII–DIV linker, the FIF/AAA mutations were engineered into $Na_V1.5$ and the behavior of the WT and mutant constructs were compared. As shown in Fig. 2*A* and Table 1, in elevated $[Ca^{2+}]_i$ the voltage-dependent inactivation of the FIF/AAA channel was indistinguishable from WT or A1924T. Furthermore, like WT or A1924T, FIF/AAA displays the typical left-shift in the inactivation curve when $[Ca^{2+}]_i$ is

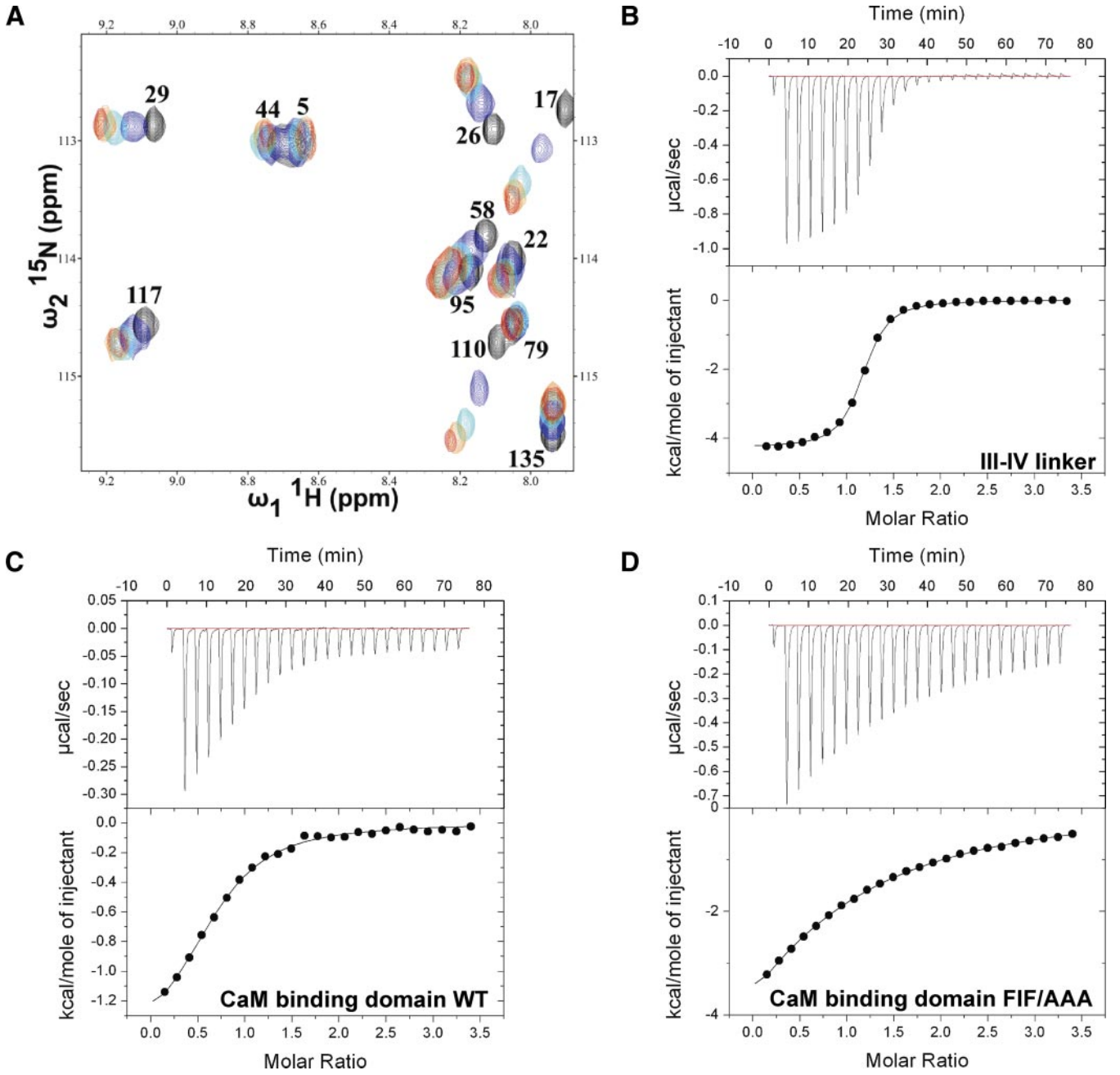

FIGURE 4. **NMR titration and isothermal titration calorimetry analysis of interactions between CaM and the III–IV linker.** *A*, overlay of ^{1}H-^{15}N HSQC NMR spectra of ^{15}N-enriched CaM at 200 μM with different concentrations of III–IV linker (*black*, 0 μM; *blue*, 50 μM; *cyan*, 100 μM; *orange*, 200 μM; and *red*, 400 μM). CaM resonance assignments were made using the entry from the BioMagResBank (code 6541). *B–D*, isothermal titration calorimetry measurements of the binding of CaM interaction to III–IV linker (*B*), WT CaM-binding domain (*C*), and FIF/AAA mutant CaM-binding domain (*D*). The *upper* and *lower panels* show the raw ITC data and a plot of the integrated area of each peak, respectively.

lowered (Fig. 2*A* and Table 1). Importantly, as we observed for A1924T, FIF/AAA displayed an even more marked left shift in $V_{½}$ of inactivation than WT (Fig. 2*A*, compare *filled* and *open squares*, and Table 1). Thus, as for the C-terminal CaM-binding motif, CaM binding to the FIF/AAA motif plays an important role in limiting the development of inactivation at low $[Ca^{2+}]_i$. Moreover, like the C-terminal A1924T mutant, FIF/AAA channel voltage-dependent inactivation was insensitive to lidocaine in elevated $[Ca^{2+}]_i$ (Fig. 2*C* and Table 1). These results suggest that these sites in the C terminus and DIII–DIV linker are coordinately regulated by Ca^{2+}-sensitive CaM binding, and involve structures that are responsive to LA. These findings are also consistent with our data demonstrating that the DIII–DIV linker binds CaM specifically and with high affinity. In combination, our findings suggest that CaM may serve as a "functional bridge" between the C terminus and the primary structure responsible for Na^+ channel inactivation: the DIII–DIV linker.

DISCUSSION

Human cardiac Na^+ channels, whereas functioning in the myocardium as the primary scaffold for cardiac conduction,

also exhibit exquisite sensitivity to a variety of intracellular mediators (26). Here, we perform electrophysiology and physical interaction studies that reveal CaM-dependent functional interactions involving the C terminus and the DIII–DIV linker, using Ca^{2+} and lidocaine as molecular probes.

A mutation in the C-terminal IQ domain (A1924T) associated with the Brugada arrhythmia syndrome (8) recapitulated effects of $[Ca^{2+}]_i$ removal on Na^+ channel inactivation and lidocaine action, supporting the dual $[Ca^{2+}]_i$ sensor role proposed for the IQ domain and a central role for CaM. Using NMR spectroscopy, a novel CaM binding site was mapped to the DIII–DIV linker inactivation particle. A number of Brugada syndrome and Long QT syndrome mutations have been mapped close to or within this domain (27, 28). Alanine substitution (FIF/AAA) within the CaM-binding domain markedly reduced CaM affinity as determined by ITC, and in $Na_V1.5$ channels eliminated lidocaine effects in the same manner as Ca^{2+} removal.

Mutations in the C-terminal IQ domain (A1924T) or the newly identified CaM-binding domain in the DIII–DIV linker (FIF/AAA) have no perceptible effects on the voltage dependence of channel inactivation at high $[Ca^{2+}]_i$ (Fig. 2*A* and Table 1). However, removing $[Ca^{2+}]_i$ with BAPTA results in a marked left shift in $V_{½}$ in both mutants (Fig. 2*A*), implying that the voltage dependence of channel inactivation is influenced by CaM binding. We have previously shown that the affinity of the WT IQ domain for CaM is decreased in the presence of Ca^{2+} (14). It is therefore not surprising that in high $[Ca^{2+}]_i$, differences in channel availability between WT and the A1924T and FIF/AAA CaM binding mutants are abolished. We also showed that the C-terminal IQ motif acts as a molecular switch between the intrinsic EF-hand domain apparatus and the extrinsic Ca^{2+} sensor, CaM (14). Mutations in the EF-hand domain have effects comparable with the A1924T mutation on inactivation and LA action (not shown). Although the direct coupling of these two Ca^{2+} sensors is unique among known Ca^{2+} signaling systems, neither the mechanism for this coupling, nor the manner in which these two Ca^{2+} sensor elements modulate inactivation are known.

The observation that CaM binding to either the DIII–DIV linker or the C terminus has similar effects on voltage dependence of channel inactivation (Fig. 2*A*) and on Ca^{2+}-dependent lidocaine action (Fig. 2, *B* and *C*) is consistent with numerous studies showing that mutations in the two cytoplasmic domains have concordant effects on the voltage dependence of inactivation, and suggests functional interaction between these regions (9, 29–31). Moreover, evidence has accumulated in support of interactions between CaM, the C terminus, and the DIII–DIV linker (13, 24).

It is noteworthy that the N-terminal portion of the CaM-binding motif in the DIII–DIV linker (Fig. 3) includes a proline residue (Pro^{1511}), which prior mutational studies have shown disrupts the interaction of the DIII–DIV linker with the $Na_V1.5$ C terminus in glutathioine *S*-transferase pull-down assays (24). Our NMR and ITC results provide definitive evidence for a Ca^{2+}-dependent interaction between CaM and the DIII–DIV linker. The fact that mutations in the IQ domain (A1924T) and the DIII–DIV linker CaM-binding domain "knock-out" the same lidocaine action without eliciting baseline effects on inactivation or $[Ca^{2+}]_i$ sensitivity confirms the critical role for CaM in channel inactivation as well as the exquisite selectivity for its effect. Our results also support the proposal that CaM serves as a functional and possibly even a structural bridge between the C terminus and the DIII–DIV linker. To fully understand the mechanism of the Ca^{2+} sensitivity of $Na_V1.5$, it is important to also consider that interactions between the C-terminal EF-hand and the IQ motif will likely impact the equilibrium of CaM binding to these cytoplasmic domains (14, 15).

Although mutations disrupting the CaM-binding domains render channels resistant to LA effects on voltage-dependent availability, it was remarkable that neither these mutations nor altering $[Ca^{2+}]_i$ modified LA-associated use-dependent block. "Use-dependent" or "phasic" block develops with sustained, repeated depolarizations. Although use dependence of Na^+ channel blocking drugs is of primary importance for the therapeutic efficacy of LA in the context of cardiac arrhythmias, it can elicit paradoxical and unwanted pro-arrhythmic side effects (4, 32–34). In addition, there is a non-rate dependent "tonic block," measured during infrequent stimulation, that causes the stabilizing "left shift" in the voltage dependence of fast inactivation we studied here (35).

A consequence of tonic block is a reduction in membrane excitability, as a larger portion of channels are fully inactivated at the resting membrane potential, and are thus unavailable to open in response to a stimulus. Some LA (*e.g.* lidocaine) produce little tonic and much use-dependent block, but the inverse can also occur (36, 37). For example, the neutral LA benzocaine acts almost exclusively through tonic block (38). To avoid the pro-arrhythmic potential of use-dependent Na^+ channel block in the development of specific therapeutic applications such as pain treatment, it will therefore be important to determine the molecular details of tonic block.

It is known that treatment with LA can exacerbate arrythmias during conditions of ischemia (32). Our previous results indicate that oxidative stress reduces I_{Na} availability (23). Treatment of $Na_V1.5$-expressing heterologous cells with the general oxidant *t*-butyl hydroperoxide (t-BHP) resulted in a −7 mV hyperpolarizing shift of the $V_{½}$ of inactivation that is reminiscent of the −8 mV shift we observe upon shifting from high to nominally Ca^{2+}-free conditions in the current study (Table 1). The rise in $[Ca^{2+}]_i$ during an ischemic event would therefore be expected to counteract the effects of oxidative damage on Na^+ channel availability and restore conduction. In contrast, application of therapeutic lidocaine following an ischemic event would be expected to aggravate the effects of oxidative damage by shifting the availability curve to the left, and counterbalance the ameliorating effects of rising intracellular $[Ca^{2+}]_i$.

To understand the potential impact of these effects on cardiac conduction, we modeled the effects of oxidation, changing intracellular $[Ca^{2+}]_i$ and LA exposure in a cable model of simulated cardiac ventricular myocytes. The results are summarized in Fig. 5, which shows action potentials from the middle of the fiber for the different conditions. The *inset* shows the upstroke at greater magnification to illustrate changes in upstroke velocity, which are a primary determinant of conduc-

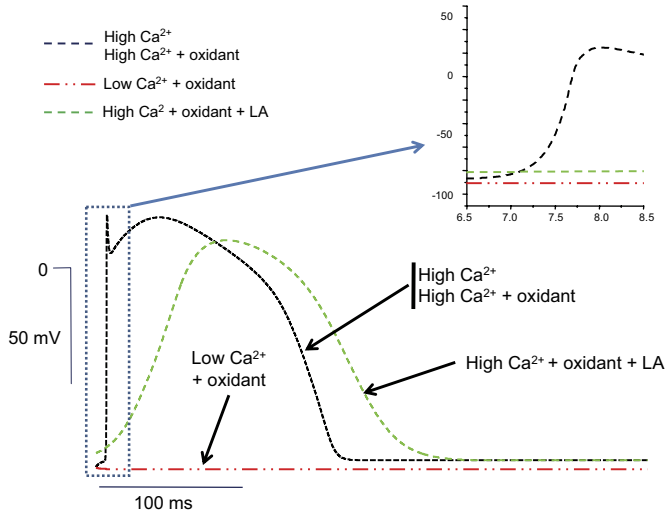

FIGURE 5. **Effects of intracellular Ca^{2+}, oxidation, and local anesthetics on action potential (*AP*) conduction using the Luo-Rudy model.** Action potentials from the middle of the one-dimensional fiber for the different conditions are overlaid to illustrate changes in action potential duration and upstroke velocity. The *inset* shows the AP upstroke at greater magnification. The conduction velocities computed from the fiber in high $[Ca^{2+}]$ (*D*), high $[Ca^{2+}]$(*D*) plus oxidant, low $[Ca^{2+}]$ (*D*) plus oxidant and high $[Ca^{2+}]$ (*D*) plus oxidant plus LA were 67, 64, 0, and 4 cm/s, respectively. The following values for the $V_{1/2}$ were used to generate the data: −71.3 mV in high $[Ca^{2+}]_i$; −75.2 mV in high $[Ca^{2+}]_i$ plus *t*-BHP; −86.7 mV in low $[Ca^{2+}]_i$ plus *t*-BHP; −80.3 mV in high $[Ca^{2+}]_i$ plus *t*-BHP plus LA.

tion velocity, and are heavily influenced by the magnitude of I_{Na}. As expected, the effects of lowering $[Ca^{2+}]_i$ or adding *t*-BHP, conditions that elicit left shifts in the Na^+ channel $V_{½}$, had a negative impact on the rate of action potential upstroke and conduction velocity in the model fiber. Conversely, elevation of $[Ca^{2+}]_i$ resulted in increased upstroke velocity and faster conduction compared with the Ca^{2+}-free condition in non-oxidative conditions (*panel A*), and had the same salutatory effect in oxidative conditions (*panel B*, compare *t*-BHP + Ca^{2+} to *t*-BHP + BAPTA). However, elevating $[Ca^{2+}]_i$ could not rescue conduction when the fiber was exposed to both LA and oxidative conditions. These simulations suggest that Ca^{2+}-dependent as well as drug-dependent modulation of Na^+ channel inactivation could critically influence conduction during oxidative stress. Heterogeneities in the action potential duration, coupled with conduction velocity changes could lead to marked dispersion of repolarization and unidirectional conduction block, especially in the ischemic myocardium and border zone, a substrate that favors the development of re-entrant arrhythmias (39, 40).

In summary, these findings suggest a functional interaction between the C terminus and the DIII–DIV linker, revealed through complementary responses to $[Ca^{2+}]_i$ and lidocaine, which is dependent on CaM. Therapeutic intervention targeted to the $[Ca^{2+}]_i$-dependent mechanisms that modulate Na^+ channel function may be a useful approach for treating genetic and pathophysiologic conditions where $[Ca^{2+}]_i$ impacts cardiac conduction.

Acknowledgment—We thank Wen Shuai for expert technical assistance.

REFERENCES

1. Viswanathan, P. C., and Balser, J. R. (2004) *Trends Cardiovasc. Med.* **14,** 28–35
2. Stuhmer, W., Conti, F., Suzuki, H., Wang, X. D., Noda, M., Yahagi, N., Kubo, H., and Numa, S. (1989) *Nature* **339,** 597–603
3. West, J. W., Patton, D. E., Scheuer, T., Wang, Y., Goldin, A. L., and Catterall, W. A. (1992) *Proc. Natl. Acad. Sci. U. S. A.* **89,** 10910–10914
4. Balser, J. R., Nuss, H. B., Orias, D. W., Johns, D. C., Marban, E., Tomaselli, G. F., and Lawrence, J. H. (1996) *J. Clin. Investig.* **98,** 2874–2886
5. Mantegazza, M., Yu, F. H., Catterall, W. A., and Scheuer, T. (2001) *Proc. Natl. Acad. Sci. U. S. A.* **98,** 15348–15353
6. Viswanathan, P. C., Bezzina, C. R., George, A. L., Jr., Roden, D. M., Wilde, A. A., and Balser, J. R. (2001) *Circulation* **104,** 1200–1205
7. Brugada, P., and Brugada, J. (1992) *J. Am. Coll. Cardiol.* **20,** 1391–1396
8. Tan, H. L., Kupershmidt, S., Zhang, R., Stepanovic, S., Roden, D. M., Wilde, A. A., Anderson, M. E., and Balser, J. R. (2002) *Nature* **415,** 442–447
9. Veldkamp, M. W., Viswanathan, P. C., Bezzina, C., Baartscheer, A., Wilde, A. A., and Balser, J. R. (2000) *Circ. Res.* **86,** E91–E97
10. Wei, J., Wang, D. W., Alings, M., Fish, F., Wathen, M., Roden, D. M., and George, A. L., Jr. (1999) *Circulation* **99,** 3165–3171
11. Opie, L. H., and Clusin, W. T. (1990) *Annu. Rev. Med.* **41,** 231–238
12. Deschenes, I., Neyroud, N., DiSilvestre, D., Marban, E., Yue, D. T., and Tomaselli, G. F. (2002) *Circ. Res.* **90,** E49–E57
13. Kim, J., Ghosh, S., Liu, H., Tateyama, M., Kass, R. S., and Pitt, G. S. (2004) *J. Biol. Chem.* **279,** 45004–45012
14. Shah, V. N., Wingo, T. L., Weiss, K. L., Williams, C. K., Balser, J. R., and Chazin, W. J. (2006) *Proc. Natl. Acad. Sci. U. S. A.* **103,** 3592–3597
15. Wingo, T. L., Shah, V. N., Anderson, M. E., Lybrand, T. P., Chazin, W. J., and Balser, J. R. (2004) *Nat. Struct. Mol. Biol.* **11,** 219–225
16. Tan, H. L., Bink-Boelkens, M. T., Bezzina, C. R., Viswanathan, P. C., Beaufort-Krol, G. C., van Tintelen, P. J., van den Berg, M. P., Wilde, A. A., and Balser, J. R. (2001) *Nature* **409,** 1043–1047
17. Vogel, H. J., Lindhal, L., and Thulin, E. (1983) *FEBS Lett.* **157,** 241–246
18. Kainosho, M., Torizawa, T., Iwashita, Y., Terauchi, T., Mei, O. A., and Guntert, P. (2006) *Nature* **440,** 52–57
19. Delaglio, F., Grzesiek, S., Vuister, G. W., Zhu, G., Pfeifer, J., and Bax, A. (1995) *J. Biomol. NMR* **6,** 277–293
20. Ong, B. H., Tomaselli, G. F., and Balser, J. R. (2000) *J. Gen. Physiol.* **116,** 653–662
21. Kambouris, N. G., Nuss, H. B., Johns, D. C., Marban, E., Tomaselli, G. F., and Balser, J. R. (2000) *J. Clin. Investig.* **105,** 1133–1140
22. Vedantham, V., and Cannon, S. C. (1999) *J. Gen. Physiol.* **113,** 7–16
23. Fukuda, K., Davies, S. S., Nakajima, T., Ong, B. H., Kupershmidt, S., Fessel, J., Amarnath, V., Anderson, M. E., Boyden, P. A., Viswanathan, P. C., Roberts, L. J., and Balser, J. R. (2005) *Circ. Res.* **97,** 1262–1269
24. Motoike, H. K., Liu, H., Glaaser, I. W., Yang, A. S., Tateyama, M., and Kass, R. S. (2004) *J. Gen. Physiol.* **123,** 155–165
25. Yap, K. L., Kim, J., Truong, K., Sherman, M., Yuan, T., and Ikura, M. (2000) *J. Struct. Funct. Genomics* **1,** 8–14
26. Catterall, W. A., Hulme, J. T., Jiang, X., and Few, W. P. (2006) *J. Recept. Signal. Transduct. Res.* **26,** 577–598
27. Smits, J. P., Eckardt, L., Probst, V., Bezzina, C. R., Schott, J. J., Remme, C. A., Haverkamp, W., Breithardt, G., Escande, D., Schulze-Bahr, E., LeMarec, H., and Wilde, A. A. (2002) *J. Am. Coll. Cardiol.* **40,** 350–356
28. Splawski, I., Shen, J., Timothy, K. W., Lehmann, M. H., Priori, S., Robinson, J. L., Moss, A. J., Schwartz, P. J., Towbin, J. A., Vincent, G. M., and Keating, M. T. (2000) *Circulation* **102,** 1178–1185
29. Baroudi, G., and Chahine, M. (2000) *FEBS Lett.* **487,** 224–228
30. Ellinor, P. T., Nam, E. G., Shea, M. A., Milan, D. J., Ruskin, J. N., and Macrae, C. A. (2008) *Heart Rhythm.* **5,** 99–105
31. Rivolta, I., Clancy, C. E., Tateyama, M., Liu, H., Priori, S. G., and Kass, R. S. (2002) *Physiol. Genomics* **10,** 191–197
32. Echt, D. S., Liebson, P. R., Mitchell, L. B., Peters, R. W., Obias-Manno, D., Barker, A. H., Arensberg, D., Baker, A., Friedman, L., and Greene, H. L. (1991) *N. Engl. J. Med.* **324,** 781–788
33. Vaughan Williams, E. M. (1989) *Am. J. Cardiol.* **64,** 5J–9J

34. Yogeeswari, P., Ragavendran, J. V., Thirumurugan, R., Saxena, A., and Sriram, D. (2004) *Curr. Drug Targets* **5,** 589–602
35. Bean, B. P., Cohen, C. J., and Tsien, R. W. (1983) *J. Gen. Physiol.* **81,** 613–642
36. Butterworth, J. F., and Strichartz, G. R. (1990) *Anesthesiology* **72,** 711–734
37. Stummann, T. C., Salvati, P., Fariello, R. G., and Faravelli, L. (2005) *Eur. J. Pharmacol.* **510,** 197–208
38. DeLuca, A., Probstle, T., Brinkmeier, H., and Rudel, R. (1991) *Naunyn Schmiedebergs Arch. Pharmacol.* **344,** 596–601
39. Pogwizd, S. M., and Corr, P. B. (1987) *Circ. Res.* **61,** 352–371
40. Robert, E., Aya, A. G., de La Coussaye, J. E., Peray, P., Juan, J. M., Brugada, J., Davy, J. M., and Eledjam, J. J. (1999) *Am. J. Physiol.* **276,** H413–H423